
Article:
Prasannakumar, V and Lloyd, GE (2007) Development of crystal lattice preferred orientation and seismic properties in Bhavani shear zone, Southern India. Journal of Geological Society of India, 70. pp. 282-296. ISSN 0016-7622

DEVELOPMENT OF CRYSTALLOGRAPHIC LATTICE PREFERRED ORIENTATION AND SEISMIC PROPERTIES IN BHAVANI SHEAR ZONE, SOUTHERN INDIA

V. Prasannakumar and Geoffrey E. Lloyd

Department of Geology, University of Kerala, Kariavattom, Trivandrum, India 695 581.

*School of Earth Sciences, University of Leeds, Leeds LS2 9JT, UK.

Abstract

Shear markers and shear sense indicators from the Bhavani shear zone (BSZ), a member of the south Indian Proterozoic shear system, separating the northern Archaean and southern Pan African granulite terranes, suggest multiphase reactivation. There is a progressive increase in mylonitisation corresponding to a progression in strain. The LS fabrics indicate near vertical principal flattening plane trending ENE-WSW, but with subvertical as well as subhorizontal stretching lineations implying a possible reactivation history with opposing movement vectors. Whilst the SEM-EBSD derived LPO of amphibole, biotite and feldspars suggest plastic deformation through the activation of intracrystalline slip systems, diffusional creep accommodated deformation can be inferred from the quartz LPO. All LPO suggest modifications in the fabric due to both retrograde and prograde reactivation during the tectono-thermal history of the BSZ over a period of nearly 2.0Ga. Petrofabric-derived seismic properties for the BSZ suggest that it exhibits a considerable seismic anisotropy, which reflects the petrofabrics of hornblende and biotite. Both LPO and seismic property observations imply conflicting tectonic X and Y directions, indicating possible superposition of contrasting X and Y vectors during different phases of the shear zone reactivation.

Keywords: microfabric, EBSD analysis, seismic anisotropy, reactivation, Bhavani shear zone, south India.

1. INTRODUCTION

Shear zones, ranging from microscopic to macroscopic scales, are the loci of ductile deformation and hence their tectono-kinematic evolution has received much attention (e.g. Ramsay 1980, Ramsay and Graham, 1970, Rutter et al. 1998). Strong crystal lattice preferred orientations (LPO) are often characteristic of shear zones and may be crucial to the understanding of deformation processes and kinematics in deformed rocks (e.g. Law, 1990, Wenk and Christie, 1991, Passchier and Trouw, 1996). Thus, the accurate determination of the crystallographic orientation of the constituent mineral phases in such rocks is an essential requirement. However, most of the

techniques available for the determination of statistically representative LPO of different minerals have limitations either due to compositional constraints as in the optical universal stage technique or other reasons (e.g. due to indistinct diffraction peaks in X-ray goniometry). Fortunately, accurate determination of LPO in polymineralic rocks is now possible via SEM electron backscatter diffraction (EBSD) (Adams et al., 1993, Prior et al., 1999). The present contribution describes the LPO in a polymineralic mylonite from the Bhavani shear zone, South India, determined via SEM EBSD, with the aim of constraining the mechanisms of development of shear zone microfabric. It is shown also how the LPO can be used to predict the seismic properties, including seismic anisotropy, of the Bhavani shear zone.

2. GEOLOGICAL SETTING

The South Indian shield (Fig. 1) comprises of a mosaic of several crustal blocks with contrasting geological and geochronological signatures ranging from Archaean to Proterozoic (Newton and Hansen, 1986; Harris *et al.,* 1994). It is dissected by two major shear systems (Drury and Holt, 1980), the Palghat-Cauvery and the Achankovil. The former, a deeply dissected section of an Archaean orogenic belt and a zone of reworking, consists of the Moyar, Bhavani, Palghat and Cauvery shear zones and acts as a terrane boundary between the early Proterozoic northern granulites of about 2.5Ga (Friend and Nutman, 1992) and the southern granulites of Pan-African age, close to 0.55Ga (Bartlet *et al.,* 1995). This major crustal discontinuity, extending for about 300km in an E-W to NE-SW direction, hosts acid to ultrabasic intrusives and has been variously treated as a fault zone (Grady, 1971), aulacogen (Katz, 1978) or suture (Janardhan *et al.,* 1994).

The Bhavani Shear Zone (BSZ) forms the northwestern boundary of the Palghat-Cauvery shear system and extends in a NE-SW direction, bordering the southern periphery of the Nilgiri charnockite massif (Fig.1). The BSZ joins with the Moyar shear zone towards the east and continues further east with a general E-W to ENE-WSW trend and exhibits both mesoscopic and microscopic features typical of deformation by ductile shearing and fabrics representing all stages of mylonitisation from protomylonite to ultramylonite. However, shear sense indicators suggest both dextral and sinistral strike-slip movements, often in the same sample. In some cases, these are clearly overprinting relationships indicating reactivation. Outcrop scale

shear zones with diverse orientations, sense of movement and overprinting relations have modified shear sense indicators such that controversy surrounds the actual sense of movement (Nair *et al*., 1981; Naha and Srinivasan 1996; Cruz *et al*., 2000; Mukhopadhyay *et al*., 2003; Jain *et al*., 2003).

2.1 Shear zones

The BSZ (Fig. 2a) is dominated by hornblende-biotite gneiss, schists and amphibolite. Highly deformed quartz-biotite schist and augen gneiss with mylonitic fabric, exposed in the central part of the zone, generally grades into hornblende-biotite gneiss on either side. The general structural grain is controlled by mutually parallel compositional layering (S_0) and foliation (S_1) striking ENE-WSW and dipping moderately-to-steeply towards the north or south (Fig. 2b). The most widely developed planar fabric is a penetrative foliation (S_1) after crystals of hornblende, flakes of biotite and flattened grains of quartz and feldspar.

Polyphase deformation has resulted in the formation of folds differing in tectonic style and orientation (Nair *et al.,* 1981). Based on geometry, orientation of hinge line and axial plane, relation with planar surfaces and nature of overprinting, folds are grouped into four (i.e. F_1, F_2, F_3, F_4; see Fig. 2b). The earliest folds (F_1) are rare and are represented as rootless folds in which S_o is transposed into parallelism with S_1 except in fold hinges. The F_2 folds are tight, asymmetrical and plunging moderately to east or west. They often exhibit axial planar foliation (S_2) defined by streaked plates of biotite, crystals of hornblende and elongated polycrystalline aggregates of quartz and feldspar and associated grain size reduction. The third group of folds (F_3) are coaxial with F_2 and deform all earlier foliations (i.e. $S_{0\text{-}2}$). In contrast to the others, the F_4 folds plunge steeply to north or south and are broad and open. Mineral lineations (L_1), defined by hornblende crystals and biotite aggregates, plunge moderately to the east or west.

A number of parallel/subparallel ductile shear/mylonite zones, trending ENE-WSW, occur within the major BSZ. These minor shear zones vary in width from tens of centimetres to tens of metres and strike extension from a few tens to hundreds of metres (Fig. 3a, b). Mylonitic to ultramylonitic fabric characterizes the bulk of the shear zone and there is a progressive increase in foliation intensity towards the

mylonitic zones. The variants correspond to a progression in strain manifested by grain size reduction and increasing flattening and elongation of polycrystalline quartz, feldspar and hornblende-biotite rich layers.

Folds of differing tectonic styles, each with axial planes and axial planar mylonitic foliations, indicate that the foliation surface is the principal flattening plane (i.e. XY, where $X \geq Y \geq Z$). All linear features (i.e. stretching lineations, groove lineations and striations on the mylonitic shear planes) are either subhorizontal-gently plunging towards ENE/WSW or moderately-to-steeply plunging to N/S. All fabric characteristics indicate that the penetrative foliation (S_1) is a product of ductile shearing and has been transposed on a pre-shear fabric (S_0). In places the mylonitic foliation is further transposed by a subparallel non-penetrative foliation (S_2), which is axial planar to the second generation folds. Although distinction between mutually parallel S-surfaces and shear planes is not possible in the ultramylonite stage, overprinting of ductile shear bands (i.e. C-surfaces) has been recognised at several places. The angle between C-surfaces and foliation (S) surfaces is >20°.

2.2 Sample description

A representative sample of the mylonitic shear zone gneiss (VPK4) was selected for detailed microstructural analysis. The sample exhibits a homogenous mineral assemblage of quartz + plagioclase + K-feldspar + amphibole + biotite, with accessory epidote, sphene, apatite, ilmenite and zircon. The amphiboles are calcic and correspond to magnesio-hornblende, which are considered to have formed under epidote-amphibolite facies conditions. The plagioclase has an andesine composition of ~An38.

The mylonite shows a differentiated microfabric in which layers of platy plagioclase and quartz alternate with green prismatic amphibole and flakes of brown biotite. Quartz typically occurs as polycrystalline aggregates, with individual grain sizes in the range 60-100μm. Quartz grain boundaries are mainly polygonal, although some are lobate and bulge into adjacent minerals. Plagioclase occurs as recrystallised strain-free grains ranging in size from 30 to 70μm that are almost equidimensional and exhibit straight as well as lobate grain boundaries. Occasionally polygonal outlines with 120^o triple junctions are seen. Hornblende occurs typically as coarse, stout

prismatic crystals elongate parallel to the stretching lineation with transgranular fractures common. However, it occurs also with a finer grain size in the polymineralic matrix, where it often forms a weak preferred dimensional orientation at an angle to the penetrative fabric. There is no difference in composition between the coarse and fine grained hornblendes. Most hornblende, biotite and K-feldspar grain boundaries have dihedral angles <60°, sometimes as low as 10°, and many hornblendes display lobate grain boundaries with plagioclase and biotite.

3. SEM EBSD ANALYSIS

Electron backscattered diffraction (EBSD) in the scanning electron microscope (SEM) is now recognized as one of the main techniques of petrofabric analysis (e.g. Prior et al. 1999). Its principal advantage is that it is capable of measuring automatically the exact crystallographic orientation of individual grains, subgrains, etc. for most minerals in polymineralic samples whilst maintaining a one-to-one relationship between orientation and microstructure (e.g. Lloyd 2004). This relationship is augmented by the ability to reproduce samples in several different types of simulated images. The most frequently used simulations are as follows. (1) 'Euler-maps' (Fig. 4a), the individual (i.e. 'raw') data for those points in the EBSD grid actually analysed, colour-coded according to their crystallographic orientation as defined by three spherical Euler angles (Bunge 1982). (2) Image processed Euler-maps (Fig. 4b), usually involving the subtraction of zero solutions ('spike removal') from the raw Euler-map and several (typically no more than three) iterations ('extrapolations') in which the solutions for neighbouring points progressively replace adjacent zero solutions (n.b. care must be taken not to introduce image analysis artefacts in to any microstructure via this process). (3) Band contrast images (Fig. 4c), a grey scale representation of the quality of the EBSD pattern at each point. (4) Phase maps (Fig. 4d), which show the distribution of minerals based on EBSD pattern indexing. Because EBSD pattern indexing involves the recognition of the specific mineral phase, EBSD analysis provides also a (sometimes crude) modal analysis. The EBSD-determined modal proportions for sample VPK4 are: quartz, 14.75%; plagioclase, 44.53%; orthoclase, 15.07%; hornblende, 16.07%; and biotite, 9.59%.

3.1 Experimental conditions

Sample VPK4 was analysed via EBSD using a *CamScan Series-4* SEM operated at 20keV and ~2.0x10^{-8}nA. The sample was tilted at 75° towards the EBSD camera and fore-scattered electron (FSE) detector. The whole of the sample was traversed by the electron beam in a 440x480 grid using a 25μm step (i.e. ~11mm x 12mm area), resulting in 211200 EBSD sampling points. However, due to the presence of a variety of sampling 'artefacts' (e.g. unrecognisable patterns, holes, dirt, grain boundaries, accessory minerals not included in the analysis, etc.) only 123795 (i.e. 58.6%) of points were actually analysed.

EBSD patterns from each point in the traverse were collected and analysed automatically via *HKL Channel5* software (Schmidt and Olesen, 1989), incorporating crystallographic and diffraction reflector databases for quartz (Laue group -3m, trigonal high), plagioclase An38 (Laue group -1, triclinic), orthoclase (Laue group 2/m, monoclinic *b* setting), hornblende (Laue group 2/m, monoclinic *b* setting) and biotite (Laue group 2/m, monoclinic *b* setting) constructed from data provided by the Inorganic Crystal Structure Database (ICSD) of the UK EPSRC Chemical Database Service (CDS).

To ensure accurate EBSD pattern recognition, a relatively strict maximum mean angular deviation (MAD) between observed and predicted patterns of 1.0 was used, rather than values of 1.3-1.5 typically used in EBSD analyses (e.g. Prior et al. 1999). However, the average value of MAD for each mineral was between 0.5 and 0.6, indicating even greater confidence in the automatic indexing procedure. Nevertheless, other problems with automatic EBSD pattern recognition do exist, particularly for lower symmetry phases such as feldspars and biotite.

Although plagioclase feldspars are centro-symmetric, such that for every lattice plane *hkl* there is a lattice plane $\overline{h}\overline{k}l$ that is equivalent for (electron) diffraction purposes, the planes are physically different if the whole crystal orientation relevant for plastic deformation is considered (Wenk et al. 1986). Thus, lower and upper hemisphere projections are not symmetrically equivalent. Unfortunately, if plagioclase orientations are considered as non-polar data, which is usual for the other symmetry classes, they result in symmetrically identical upper and lower hemisphere projections that fail to describe the orientation distributions completely (e.g. Fig. 5c, d). It is necessary therefore to consider plagioclase orientations as polar data, which results in

an accurate representation of the orientation distributions provided that both the upper and lower hemisphere projections are plotted (Fig. 5a, b). In spite of these precautions, it may be difficult-to-impossible to distinguish between some plagioclase patterns and their axial equivalents via EBSD analysis, resulting in so-called pseudo-symmetry artefacts in the pole figure orientation distributions (e.g. Prior et al. 1999).

In contrast, whilst biotite does not suffer from the plagioclase problem described above, it yields typically poor to indistinct/absent EBSD patterns, particularly where the incident electron beam is (sub)parallel to cleavage planes. Patterns from cleavage surfaces *may* have better quality. As the quality of the pattern decreases, it is increasingly likely that the observed pattern will be either mis-indexed or not indexed at all.

To ensure the veracity of the automatically indexed EBSD patterns, a small-scale manual EBSD analysis of sample VPK4 was performed. The results were similar to those obtained via automated analysis (see below), albeit with much reduced sampling statistics.

3.2 Petrofabrics

Crystal lattice preferred orientation (LPO) pole figures for the conventional directions and planes for each of the minerals were calculated using software developed by Mainprice (2003). The orientations are represented in lower hemisphere equal-area projections (except for plagioclase, for which the upper hemisphere projection must be plotted also) in which the plane of projection is XZ ($X \geq Y \geq Z$), with X (east-west) and Z (north-south). The mylonitic stretching lineation is parallel to X, whilst the foliation is vertical and trends E-W such that Y is perpendicular to the plane of projection and hence lies at the centre of the LPO pole figures. The pole figures for each mineral are shown in Figs. 5 and 6. The strength of each pole figure distribution can be indicated by its pfJ-value, although this is not to be confused with the J-index, which indicates the strength of the overall mineral LPO (Bunge 1982). A pfJ-value of 1.0 indicates a random distribution. In general, the strongest LPO are shown by the hornblende and biotite and whereas the orthoclase LPO is significantly stronger than plagioclase, quartz is uncharacteristically very weak (Figs. 5 and 6).

Plagioclase LPO show a distinct maximum in (001) sub-normal to the foliation in

both hemispheres (Fig. 5a, b). However, the [100] and (010) distributions are less clear due to the need to consider both hemispheres, although there does appear to be a tendency for the maxima in (010) to develop close to X and for both to occur close to the foliation. The LPO suggest therefore crystal slip on (001)[010], which appears not to have been recognised as a common slip system in feldspars, although the orthoclase LPO (see below) suggest also [010] as a slip direction. In contrast, dislocation glide on (010)[001] and (010)[100] slip systems is considered to be the main mechanism for LPO development in plagioclase at high temperature (Egydio-Silva et al. 2002), whilst a maximum in [100] parallel to X is thought to be consistent with high grade metamorphism (Kruhl 1987, Dornbush et al. 1994). LPO with (010) subparallel to foliation and [100] and [001] sub-parallel to Y and X respectively provide indirect evidence for dislocation glide on the (010)[100] and (010)[001] slip systems (Olsen & Kohlstedt 1984, Ji and Mainprice, 1988a, b).

Orthoclase LPO are characterised by strong concentration of [100] close to Z, suggesting the orientation of (100) planes subparallel to the foliation, although there is a suggestion also of a diffuse girdle distribution subparallel to YZ (Fig. 6a). Both (001) and (010) are more dispersed. The former define a nearly complete great circle girdle distribution subparallel to the foliation, with a maximum subparallel to Y. The latter define a maximum subparallel to X but also show dispersions that might suggest girdle distributions subparallel to both XY and YZ. The LPO are suggestive of crystal slip on either (100)[010] and/or perhaps also (100)[001], although neither system appears to be common in feldspars(?).

Hornblende exhibits a strong LPO with (100) parallel to Z and [001] defining a girdle distribution parallel to the foliation (Fig. 6b). In contrast, (010) are more dispersed, although a weak girdle parallel to foliation is evident. The LPO is similar to others observed in middle-to-high grade metamorphic rocks (e.g. Schwerdtner, 1964, Ji and Mainprice, 1990). As (100) and [001] coincide with the flow plane and flow direction respectively, this fabric is consistent with activation of the (100)[001] slip system (e.g. Dollinger and Blacic 1975, Rooney et al. 1975, Reynard et al. 1989, Skrotzki 1990, Ji et al. 1993, Egydio-Silva et al. 2002). However, by analogy with the olivine fabric data base described by Ben Ismail & Mainprice (1998), the LPO could be described as a (100)-fibre texture and hence may indicate also slip on (100)[010].

Biotite exhibits the strongest LPO of all the minerals in the sample (Fig. 6c). There is a well-defined peripheral maximum of [001] parallel to Z and normal to the XY plane. The (001) cleavage plane of biotite typically defines the foliation plane and both (100) and (010) are constrained to lie within this plane, forming a common great circle girdle distribution. However, there is no maximum in either [100] or [010] associated with X. Rather, it appears that [110] is aligned subparallel to X, which suggests that biotite deformed via crystal slip on (001)[110].

Quartz LPO is weak, as indicated by pfJ-values that are only slightly greater than unity (Fig. 6d). However, (0001) exhibits two distinct maxima, one sub-parallel to Z and the other plunging shallowly towards WNW, whilst $(2\bar{1}\bar{1}0)$ and $(10\bar{1}0)$ appear to define weak girdle distributions sub-parallel to the foliation, with the maximum in the former subparallel to X. It is possible that the two (0001) orientations represent 'S' and 'C' fabric components (e.g. Lister & Snoke 1984) Although deformation experiments on quartz single crystals have revealed a considerable number of glide systems (e.g. Lister et al. 1978), the number of activated glide systems in naturally deformed quartz appears limited to systems that exploit the crystallographic <a> direction (Schmid and Casey 1986). It has been suggested also, on the basis of fabric simulations (e.g. Bouchez 1978, Burg and Laurent 1978, Bouchez et al, 1979), that the <a> direction tends to become aligned parallel to the direction of bulk simple shear deformation. Unfortunately, due to the unusually weak LPO, it is not possible to determine the likely crystal slip system(s), except to suggest that the observed LPO is compatible with the frequently observed basal-<a> system, although prism-c slip may be indicated also and is indicative of deformation at high temperatures. Alternatively, given the 60-100μm grain size and polygonal grain boundaries with indications of grain boundary migration, it is possible that quartz deformed by diffusion rather than dislocation creep processes, which explains the weak LPO, and subsequently annealed.

4. SEISMIC PROPERTIES

A number of factors may produce elastic anisotropy in rocks, such as spatial distribution of mineral phases, layering, grain size and shape, grain boundaries and oriented pores or fractures (e.g. Kern & Wenk 1985; Mainprice et al. 2003). However, because the majority of rock-forming minerals are elastically anisotropic, LPO

induced by deformation processes such as dislocation creep may be responsible for the bulk elastic anisotropy (e.g. Christensen 1966). Petrophysical properties, such as seismic velocities, therefore are often highly anisotropic in bulk rock aggregates (e.g. Babuska & Cara 1991).

Understanding of the cumulative impact of each microstructural variable on elastic anisotropy is obtained typically from experimental measurements or theoretical models (e.g. Burlini & Kern 1994; Wendt et al. 2003). However, the seismic properties of a rock aggregate can be calculated also from individual crystal orientation measurements, incorporating the single crystal elastic constants and LPO for each mineral weighted according to modal content (e.g. Mainprice & Humbert 1994). The seismic phase velocities and anisotropies then can be calculated in every direction (e.g. Mainprice & Silver 1993).

4.1 Methodology

The methodology used in this contribution to calculate whole rock seismic properties follows that described by Lloyd & Kendall (2004). The LPO for each mineral (i.e. as determined by EBSD and represented by Figs. 5 and 6 is combined with the respective individual single crystal elastic stiffness matrix (Table 1a) to produce an overall stiffness matrix for each mineral (Table 1b), assuming the Voight-Reuss-Hill averaging (Voigt 1928, Reuss 1929, Hill 1952). These are then combined according to the EBSD estimated modal proportions to produce an elastic stiffness matrix and density for the rock aggregate (Table 1c). Finally, the data are input in to the Christoffel equation (e.g. Nye 1957) to calculate the seismic properties in three dimensions. The Christoffel equation has three possible solutions representing the velocities of one compressional (Vp) and two shear (Vs_1, Vs_2) waves, from which the anisotropy of these waves (i.e. AVp, AVs_1 and AVs_2 respectively) as well as the overall anisotropy of the shear waves (AVs), also known as shear wave splitting, can be determined (e.g. Mainprice & Silver 1993). The actual process of producing the seismic properties utilises the suite of programs published by Mainprice (2003).

4.2 Results

In spite of being the result of the cumulative effects of five individual and different mineral LPO, the bulk rock seismic properties of sample VPK4 are remarkably simple

(Fig. 7a). The fastest Vp velocities (i.e. ~6 km/s) occupy a broad girdle parallel to foliation, with the absolute maximum in Vp subparallel to Y, whilst the slowest Vp velocities (i.e. ~5.7 km/s) are subnormal to foliation (i.e. subparallel to Z). Similar behaviour is exhibited by Vs_1, although velocities are obviously less (i.e. between 3.25 and 3.58 km/s). However, Vs_2 shows somewhat opposite behaviour, with slowest velocities (i.e. ~3.2 km/s) both parallel and normal to foliation and fastest velocities (i.e. ~3.4 km/s) occupying small circle distributions plunging moderately about the foliation normal (i.e. Z). Whilst all three waves exhibit considerable anisotropy (i.e. AVp = 6.9%, Vs_1 = 9.7% and Vs_2 = 6.0%), the opposite behaviours of the two shear waves result in considerable shear wave splitting in this rock (i.e. AVs = 10.24%). The highest values of AVs (i.e. >8%) define a girdle distribution parallel to foliation, whilst very low values (i.e. <2%) occupy a broad region about the normal to foliation. Finally, the polarisation of the fast shear wave (Vs_1) clearly reflects also the presence of the foliation.

The origin of the whole rock seismic properties (Fig. 7a) can be explained by considering the seismic properties of each mineral individually. This is achieved by calculating the seismic properties from the LPO for each mineral whilst assuming a 100% modal content. Results are shown in Fig. 7b-f. It is clear that the whole rock seismic properties (Fig. 7a) are controlled mainly by the LPO and seismic properties of hornblende and biotite (Fig. 7d, e), although both of these minerals alone would be responsible for greater velocities and anisotropy, particularly biotite (i.e. AVs = 47%). However, in detail the whole rock seismic distributions reflect also the presence of the plagioclase LPO (Fig. 7b), particularly for Vs_2 and AVs. Indeed, although the plagioclase LPO is complex due to the need to consider both hemispheres (Fig. 5a, b), the plagioclase seismic property distributions are relatively simple. This reflects the fact that the elastic stiffness matrix derived from the plagioclase LPO is centro-symmetric and so the problems associated with plagioclase crystallography discussed above do not impact on the derivation of the seismic properties. Finally, the position of the absolute maximum in whole rock Vp is mimicked by all of the minerals, including orthoclase and quartz (Fig. 7c, f).

5. DISCUSSION

5.1 Tectonic framework of the BSZ

The analysis of gneissose microstructures and petrofabrics in sample VPK4 provides information on the mechanical behaviour of the constituent minerals during mylonitic shear zone development. The LPO of amphibole, biotite and feldspars (Figs. 5 and 6) suggest that these minerals have been deformed plastically through the activation of intracrystalline slip systems characteristic of medium to high temperature conditions. The pole figures are characteristic of dislocation creep with the activation of the (100)[001] and perhaps also (100)[010] slip systems in amphibole, the (001)[110] slip system in biotite and the (001)[010] slip system in plagioclase. In contrast, the quartz LPO is uncharacteristically weak and may represent annealing of a microstructure that developed via diffusional rather than dislocation creep processes following significant grain size reduction and subsequent annealing. Alternatively, it may represent a combination of fabrics developed in different deformation events such that quartz LPO of the mylonite is characterised by reduction of LPO intensity compared to the protolith. The general tectonic set up of the BSZ rocks indicates polyphase deformation and metamorphism suggesting retrograde as well as prograde reactivation of the shear zone. Hence it is probable that the fabric and LPO reflect the modifications by these events with one of the event dominating in the fabric development. The BSZ consists mainly of greenschist to amphibolite facies mylonites and protomylonites exhibiting both mesoscopic and microscopic features typical of deformation by ductile shearing. The tectono-metamorphic evolution of terrains to the north and south of the Palghat-Cauvery shear system suggests substantial north-side-up movements across the shear zone during the Proterozoic, with movements in the opposite sense in the Pan-African to exhume granulites of that age to the south. These movements were accompanied by strike–slip motion of unknown extent. The strike-slip movements during the polyphase reactivation history of the shear zone over a period of nearly 2.0Ga possibly have opposing vectors contributing to the ambiguity in shear sense determinations.

5.2 Seismic framework of the BSZ

If sample VPK4 is characteristic of the BSZ, then the seismic properties of the shear zone, as predicted from the LPO of the constituent minerals, are very distinctive. In particular, the foliation should be clearly visible on seismic sections provided that a sufficient thickness of rock with these LPO is present. It is clear also that such shear

zones are capable of making a strong contribution to the seismic anisotropy of the crust, in contrast to the general assumption that the crust is seismically heterogeneous. However, in the example described, the orientation of the tectonic X direction is unclear from the seismic modelling. Indeed, the results (Fig. 7) seem to indicate a conflict between the X and Y directions. This may be real or it may indicate superposition of different X directions associated with different deformation phases.

6. CONCLUSIONS

The general tectonic milieu of the BSZ rocks suggests polyphase deformation and metamorphism with multistage reactivation of the shear zone in tune with the exhumation of the terranes to the north and the south. The opposing shear sense indicators are products of overprinting relations produced during reactivation. The centimetre to metre scale shear zones with progressive increase in foliation intensity towards the high strain zones indicate strain progression. LPO indicate microfabric features characteristic of combination of fabrics of different deformation events. The principal stretching direction as derived from the mesoscopic and microscopic structures along with LPO and seismic pole figures point to conflicting X and Y directions. Exhumation of the northern and southern blocks warrants north-side-up movements across the shear zone during the Proterozoic, with movements in the opposite sense in the Pan-African. These reactivated movements accompanied by strike-slip motion can cause conflicting X and Y vectors as in the present case. More detailed and systematic analysis of the BSZ is required to unravel this conundrum.

Acknowledgments-We thank the following for their assistance in this study: the ACU, UK and UGC, India, for the award of a Commonwealth Academic Staff Fellowship (Prasannakumar); the UK NERC for funding part of the automated EBSD system (Grant GR9/3223 to Lloyd); the UK Inorganic Crystal Structure Database (ICSD), Chemical Database Service (CDS); and David Mainprice for use of his LPO and seismic property calculation and plotting programs.

REFERENCES

Adams, B.L., Wright, S.I. & Kunze, K. 1993. Orientation imaging: the emergence of a new microscopy. *Metallurgical Transactions* 24A, 819-831.

Babuska, V. and Cara, M. 1991. *Seismic Anisotropy in the Earth*. Kluwer Academic, Dordrecht. 217pp.

Bartlet, J.M., Harris, N.B.W., Hawkesworth, C.J., & Santosh, M., 1995. New isotope constraints on crustal evolution of southern India and Pan-African metamorphism. Memoir Geological Society of India, 34, 391-397.

Ben Ismail, W. and Mainprice, D. 1998. An olivine fabric database: an overview of upper mantle fabrics and seismic anisotropy. *Tectonophysics* **296**, 145-158.

Bouchez, J.L. 1978. Preferred orientation of quartz (a)-axes in some tectonites – kinematic inferences. *Tectonophysics* 49, T25-T30.

Bouchez, J.L., Dervin, P., Mardon, J.P. and Englander, M. 1979. Neutron-diffraction applied to lattice preferred orientation study in quartzites. *Bulletin de Mineralogie* 102, 225-231.

Bunge, H.J. 1982. *Texture Analysis in Materials Science*. Butterworths, London, 599pp.

Burg, J.P. and Laurent, P. 1978. Strain analysis of a shear zone in a granodiorite. *Tectonophysics* 47, 15-42.

Burlini, L. and Kern, H. 1994. Special Issue: Seismic properties of crustal and mantle rocks - Laboratory measurements and theoretical calculations. *Surveys in Geophysics* **15**, 439-672.

Christensen, N.I. 1966. Elasticity of ultrabasic rocks. *Journal of Geophysical Research* 71, 5921-5931.

Cruz., E.D., Nair, P.K.R., & Prasannakumar, V., 2000. Palghat Gap- a dextral shear zone from the south Indian granulite terrain. Gondwana Research, 3, 21-31.

Dollinger, G. and Blacic, J.D., 1975. Deformation mechanisms in experimentally and naturally deformed amphiboles. Earth Planet. Sci. Lett., 26, 409-416.

Dornbush, H.J., Weber, K. and Skrotski, W., 1994. Development of microstructure and texture in high temperature mylonites from the Ivrea zone, In: Bunge, H.J., Segesmond, S., Skrotski, W., and Weber, K.(eds) Textures of geological materials. DGM Informations, Oberusel, 187-201.

Drury, S.A., & Holt R.W., 1980. The tectonic framework of the south Indian craton: a reconnaissance involving Landsat imagery. Tectonophysics, 65, T1-T5.

Egydio-Silva, M., Vauchez, A., Bascou, J. and Hippertt, J. 2002. High-temperature deformation in the Neoproterozoic transpressional Ribeira belt, southeast Brazil. *Tectonophysics* 352, 203-224.

Friend, C.R.L. and Nutman, A.P. 1992. Response of zircon U-Pb isotopes and whole rock geochemistry to CO_2 fluid-induced granulite facies metamorphism, Kabbaldurga, Karnataka, South India. *Contributions to Mineralogy and Petrology* 111, 299-310.

Grady, J.C. 1971. Deep main faults in South India. *Journal Geological Society India*

12, 56.

Harris, N.B.W., Santosh, M. and Taylor, P.N. 1994. Crustal evolution in South India – constraints from Nd isotopes. *Journal of Geology* 102, 139-150.

Hill, R. 1952. The elastic behaviour of a crystalline aggregate. *Proceedings of the Physical Society, London A* 65, 351-354.

Inorganic Crystal Structure Database (ICSD), Chemical Database Service (CDS). http://cds.dl.ac.uk/

Jain, A.K., Singh, S., & Manickavasagam, R.M., 2003. Intracontinental shear zones in the southern granulite terrain: their kinematics and evolution. Memoir Geological Society of India, 50, 225-253.

Janardhan, A.S., Jayanada, A.M. and Shankara, M.A. 1994. Formation and tectonic evolution of granulites from the Biligiri Rangan and Niligiri Hills, S. India – geochemical and isotopic constraints. *Journal Geological Society India* 44, 27-40.

Ji, S.C. and Mainprice, D. 1988a. Sense of shear in high temperature moevemnet zones from the fabric asymmetry of plagioclase feldspars. *Journal of Structural Geology* 10, 73-81.

Ji, S.C. and Mainprice, D. 1988b. Natural deformation fabrics of plagioclase – implications for slip systems and seismic anisotropy. *Tectonophysics* 147, 145-163.

Ji, S.C. and Mainprice, D. 1990. Recrystallisation and fabric development in plagioclase. *Journal of Geology* 98, 65-79.

Ji, S.C., Salisbury, M.H. and Hanmer, S. 1993. Petrofabric, P-wave anisotropy and seismic reflectivity of high grade tectonites. *Tectonophysics* 222, 195-226.

Katz, M.B. 1978. Tectonic evolution of Archaean granulite facies belt Sri Lanka – South India. Journal Geological Society India 19, 185-205.

Kern, H. and Wenk, H-R. 1985. Anisotropy in rocks and the geological significance. In: Wenk, H-R. (Ed.) Preferred orientation in deformed metals and rocks: an introduction to modern texture analysis, Academic Press, Orlando, 537-555.

Kruhl, J.H. 1987. Preferred lattice orientations of plagioclase from amphibolite and greenschist facies rocks near the Insubric Line (Western Alps). *Tectonophysics* 135, 233-242.

Law, R.D. 1990. Crystallographic fabrics; a selective review of their applications to research in structural geology. In, Knipe, R. J. and Rutter, E. H. (eds) , *Deformation mechanisms, rheology and tectonics*, Geological Society Special Publications **54**, 335-352.

Lister, G.S., Paterson, M.S. and Hobbs, B. E. 1978. The simulation of fabric development in plastic deformation and its application to quartzite; the model. *Tectonophysics* **45**, 107-158.

Lister, G.S. and Snoke, A.W., 1984. S-C mylonites. Jour. Struct. Geology. V.6, pp 617-638.

Lloyd, G.E. 2004. Microstructural evolution in a mylonitic quartz simple shear zone: the significant roles of dauphine twinning and misorientation. In: Alsop, G.I., Holdsworth, R.E., McCaffrey, K. and Hand, M. (eds) *Transports and Flow*

Processes in Shear Zones, Geological Society, London, Special Publications, **224**, 39-61.

Lloyd, G.E. and Kendall, J-M. 2005. Petrofabric derived seismic properties of a mylonitic quartz simple shear zone: implications for seismic reflection profiling. In: Harvey, P.K., Brewer, T., Pezard, P.A. and Petrov, V.A. (eds), *Petrophysical Properties of Crystalline Rocks*, Geological Society, London, Special Publications **240**, 75-94.

Mainprice, D. 2003. World Wide Web Address: http://www.isteem.univ-montp2.fr/TECTONOPHY/petrophysics/software/petrophysics_software.html.

Mainprice, D. and Humbert, M. 1994. Methods of calculating petrophysical properties from lattice preferred orientation data. *Survey Geophysics* 15, 575-592.

Mainprice, D. and Silver, P.G. 1993. Interpretation of SKS waves using samples from the subcontinental lithosphere. *Physics of Earth and Planetary Interiors* 78, 257-280.

Mainprice, D., Popp, T., Gueguen, Y., Huenges, E., Rutter, E.H., Wenk, H-R. and Burlini, L. 2003. Physical Properties of Rocks and other Geomaterials, a Special Volume to honour Professor H. Kern. *Tectonophysics* 370, 1-311.

Mukhopadhyay, D., Kumar, P.S., Srinivasan, R., & Bhattacharya, T., 2003. Nature of Palghat-Cauvery lineament in the region south of Namakkal, Tamilnadu,: implications for terrane assembly in south Indian granulite province. Memoir Geological Society of India, 50, 279-296.

Naha, K., & Srinivasan, R., 1996. Nature of the Moyar and Bhavani shear zones, with a note on its implications on the tectonics of the southern Indian Precambrian shield. Proceedings of the Indian Academy of Science, 105, 173-189.

Nair, P.K.R., Prasannakumar, V., & Thomas Mathai., 1981. Structure of the western termination of the Bhavani lineament. Journal of the Geological Society of India, 22, 285-291.

Newton, R.C., & Hansen, E.C., 1986. The south India-Sri Lamka high grade terrain as a possible deep crust section. In- The nature of the lower continental crust, (Ed.) Dawson, J.B., Carswell, D.A., Hall, J., Wedepohl, K.H., Geological Society Special Publication 24, 297-307.

Nye, J.F. 1957. Physical properties of crystals. Clarendon press, Oxford. 322p.

Olsen, T.S. and Kohlstedt, D.L. 1984. Analysis of dislocations in some naturally deformed plagioclase feldspars. *Physics and Chemistry of Minerals* **11**, 153-160.

Passchier, C.W., and Trouw, R.A.J., 1996. Microtectonics. Springer-Verlag, Berlin. P.289.

Prior, D.J., Boyle, A.P., Brenker, F., Cheadle, M.C., Day, A., Lopez, G., Potts, G.J., Reddy. S., Spiess, R., Timms, N., Trimby, P. Wheeler, J. & Zetterstrom, L. 1999. The application of electron backscatter diffraction and orientation contrast imaging in the SEM to textural problems in rocks. *American Mineralogist* 84, 1741-1759.

Ramsay, J.G. 1980. Shear zone geometry: a review. *Journal of Structural Geology* 2, 83-100.

Ramsay, J.G. & Graham, R.H. 1970. Strain variation in shear belts. *Canadian Journal*

of Earth Sciences 7, 786-813.

Reuss, A. 1929. Berechnung der Fließgrenze von Mischkristallen auf Grund der Plastizitätsbedingungen fur Einkristalle. *Zeitschrift für Angewandte Mathematik und Mechanik* 9, 49-58.

Reynard, B., Gillet, P. and Willaime, C. 1989. Deformation mechanisms in naturally deformed glaucophanes – a TEM and HREM study. *European Journal of Mineralogy* 1, 611-624.

Rooney, T.P., Riecker, R.E. and Gavasci, A.T. 1975. Hornblende deformation features. *Geology* 3, 364-366.

Rutter, E.H., Boriani, A., Brodie, K.H. & Burlini, L. 1998. *Special Issue*: Structures and properties of high strain zones in rocks. *Journal of Structural Geology* 20, 200pp.

Schmid, S. M., & Casey, M., 1986. Complete fabric analysis of some commonly observed quartz c axis patterns. In Heard, H. C., Hobbs, B. E., (Eds) Mineral and rock deformation, Lab. Studies- the Patterson volume. Geophys. Monograph. 36. Am. Geophys. Union. 263-286.

Schmidt, N.H. & Olesen. N.Ø. 1989. Computer-aided determination of crystal-lattice orientation from electron channelling patterns in the SEM. *Canadian Mineralogist* 27, 15-22.

Schwerdtner, W.M. 1964. Preferred orientation of hornblende in a banded hornblende gneiss. *American Journal of Science* **262**, 1212-1229.

Skrotzki, W. 1990. Microstructure in hornblende of a mylonitic amphibolite. In, Knipe, R. J. and Rutter, E. H. (eds) , *Deformation mechanisms, rheology and tectonics*, Geological Society Special Publications **54**, 321-325.

Voigt, W. 1928. Lehrbuch der Kristallphysik: mit Ausschluss der Kristalloptik. B.G. Teubner, Leipzig. 978p.

Wendt, A.S., Wirth, R., Bayuk, I.O., Covey-Crump, S.J. and Lloyd, G.E. 2003. An Experimental and Numerical Study of the Microstructural Parameters Contributing to the Seismic Anisotropy of Rocks. *Journal of Geophysical Research* 108(B8), 2365, doi:10.1029/2002JB001915.

Wenk, H-R., and Christie, J.M. 1991. Comments on the interpretation of deformation textures in rocks. *Journal of Structural Geology* **13**, 1091-1991.

Wenk, H-R., Bunge, H-J., Jansen, E. and Pannetier, J. 1986. Preferred orientation of plagioclase – neutron diffraction and U-stage data. Tectonophysics 126, 271-284.

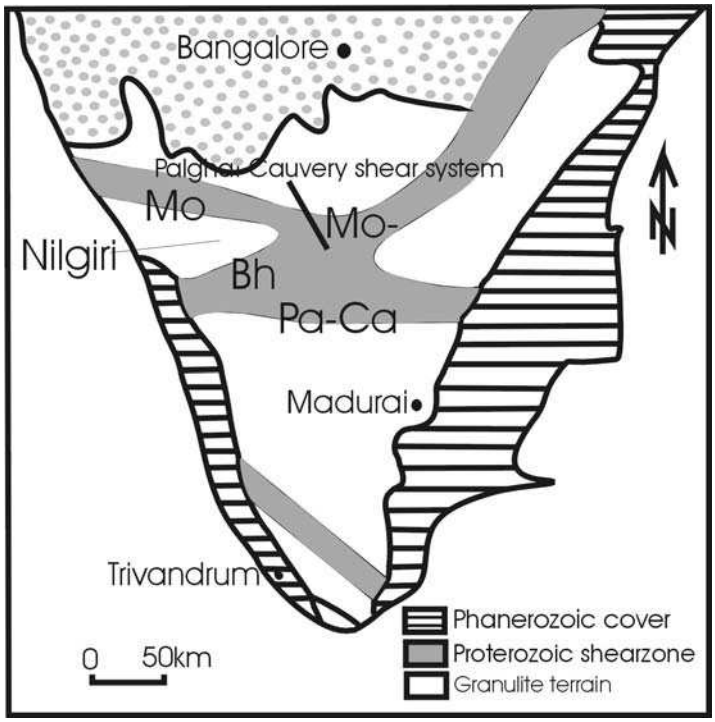

Figure 1. Simplified geology of the southern Indian shield (modified after Harris et al., 1994), showing the major shear zones considered in this study (Mo, Moyar; Bh, Bhavani; Pa-Ca, Palghat-Cauvery).

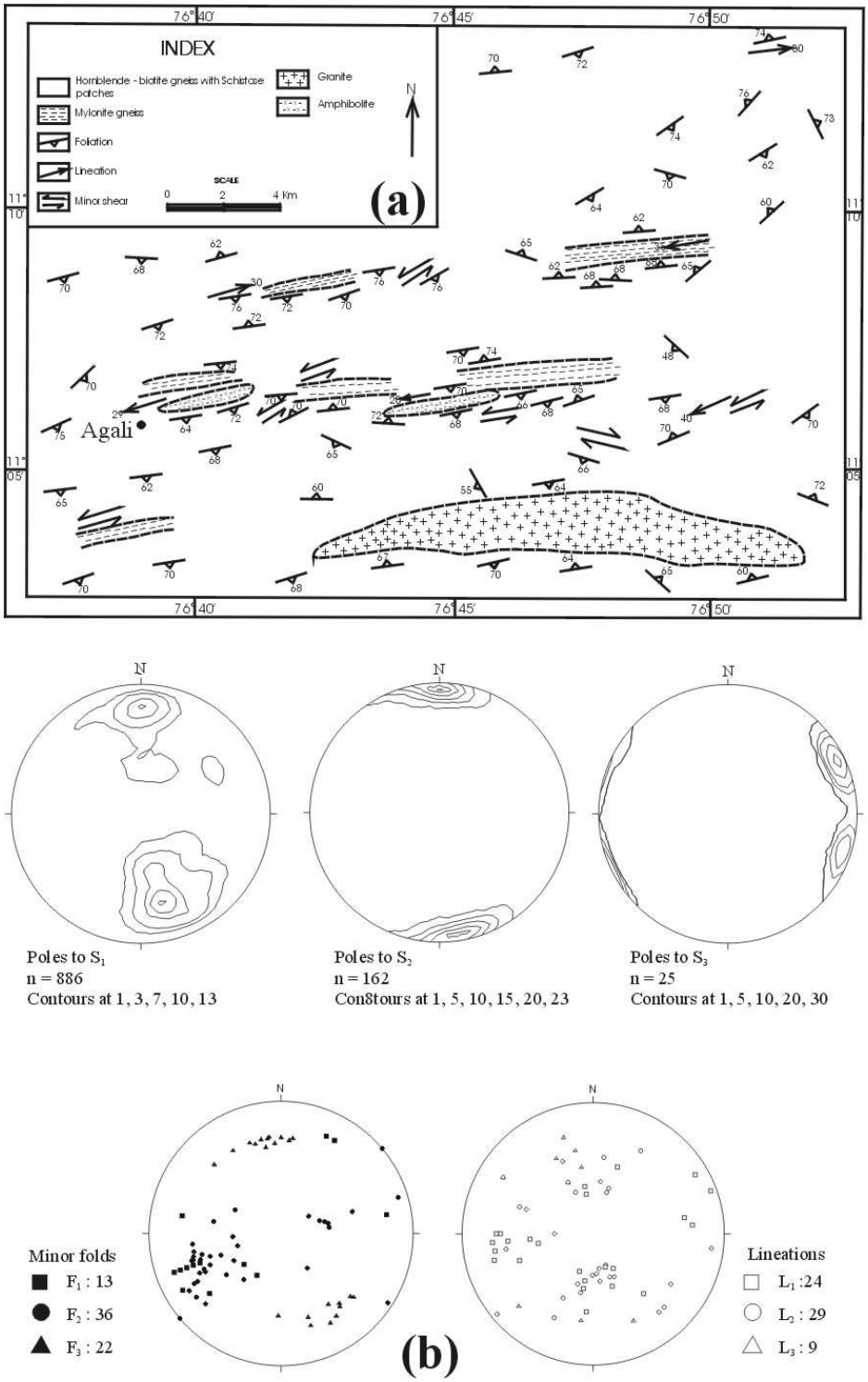

Fig. 2

Figure 2. The Bhavani shear zone. (a) Geological map indicating main lithologies and structures present. (b)Stereographic projection summarising the main structural elements (S_{0-4}, foliations; F_{1-4}, fold axes; L_{1-4}, lineations).

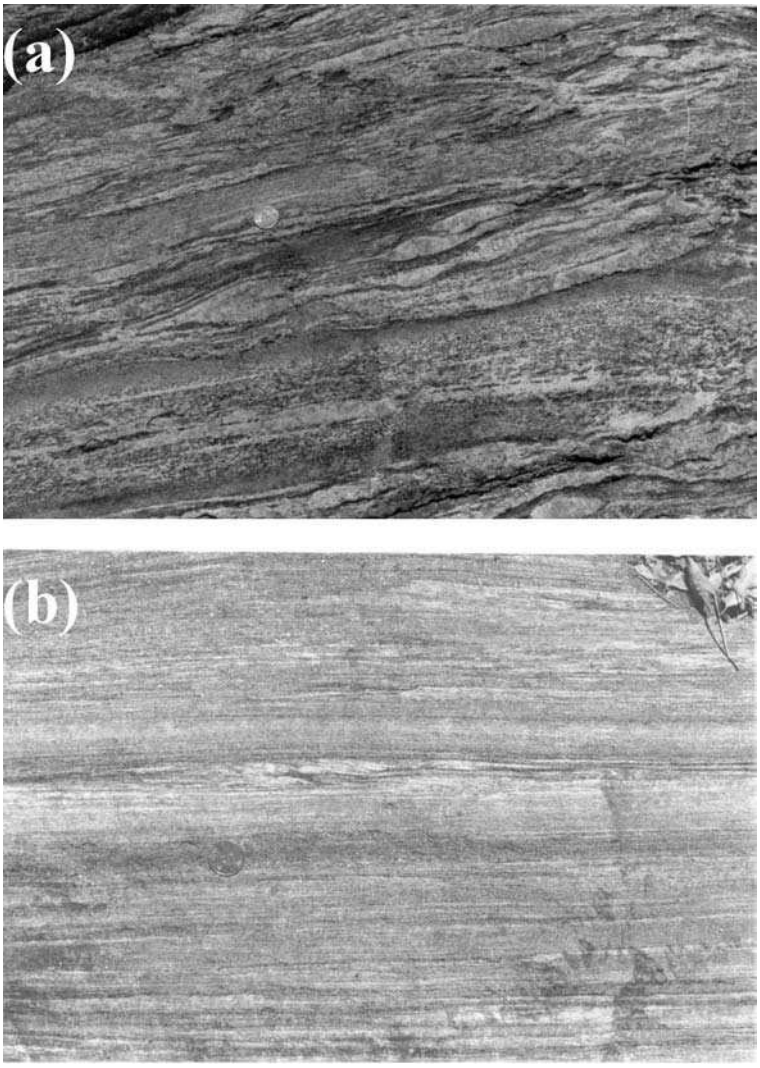

Figure 3. Examples of minor mylonitic shear zones that occur within the major Bhavani shear zone. (a) Stretched and sheared minor folds in mylonite. (b) Mylonite with stretched and flattened quarzo-felspathic layers

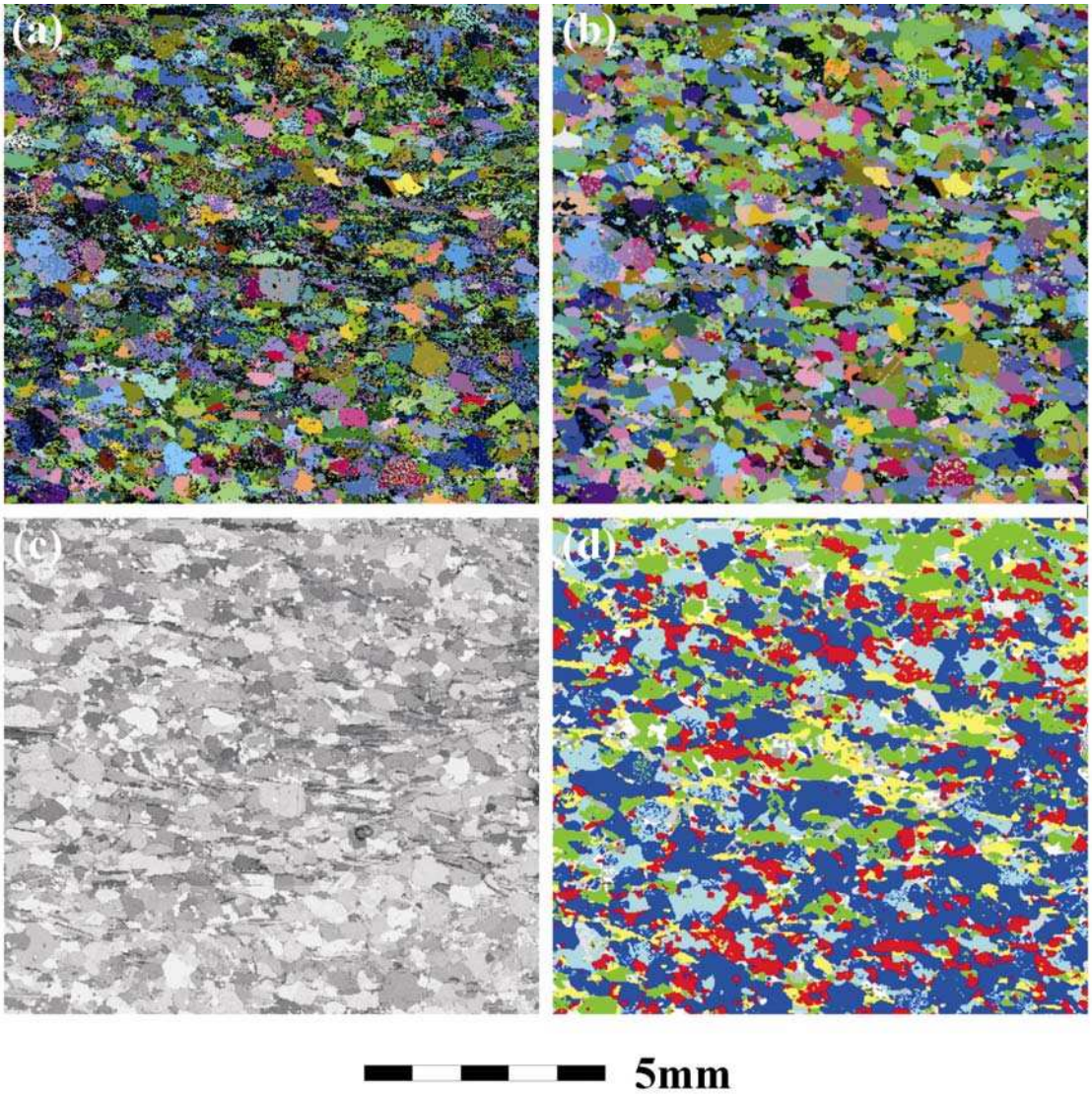

Fig. 4

Figure 4. SEM EBSD images of sample VPK4. (a) Raw Euler-map, colour-coded in terms of crystal orientation only. (b) Processed (single spike removal and 3 extrapolations) Euler-map, colour-coded in terms of crystal orientation only. (c) Band contrast image. (d) Phase image: red, quartz; dark blue, plagioclase; light blue, orthoclase; green, hornblende; yellow, biotite.

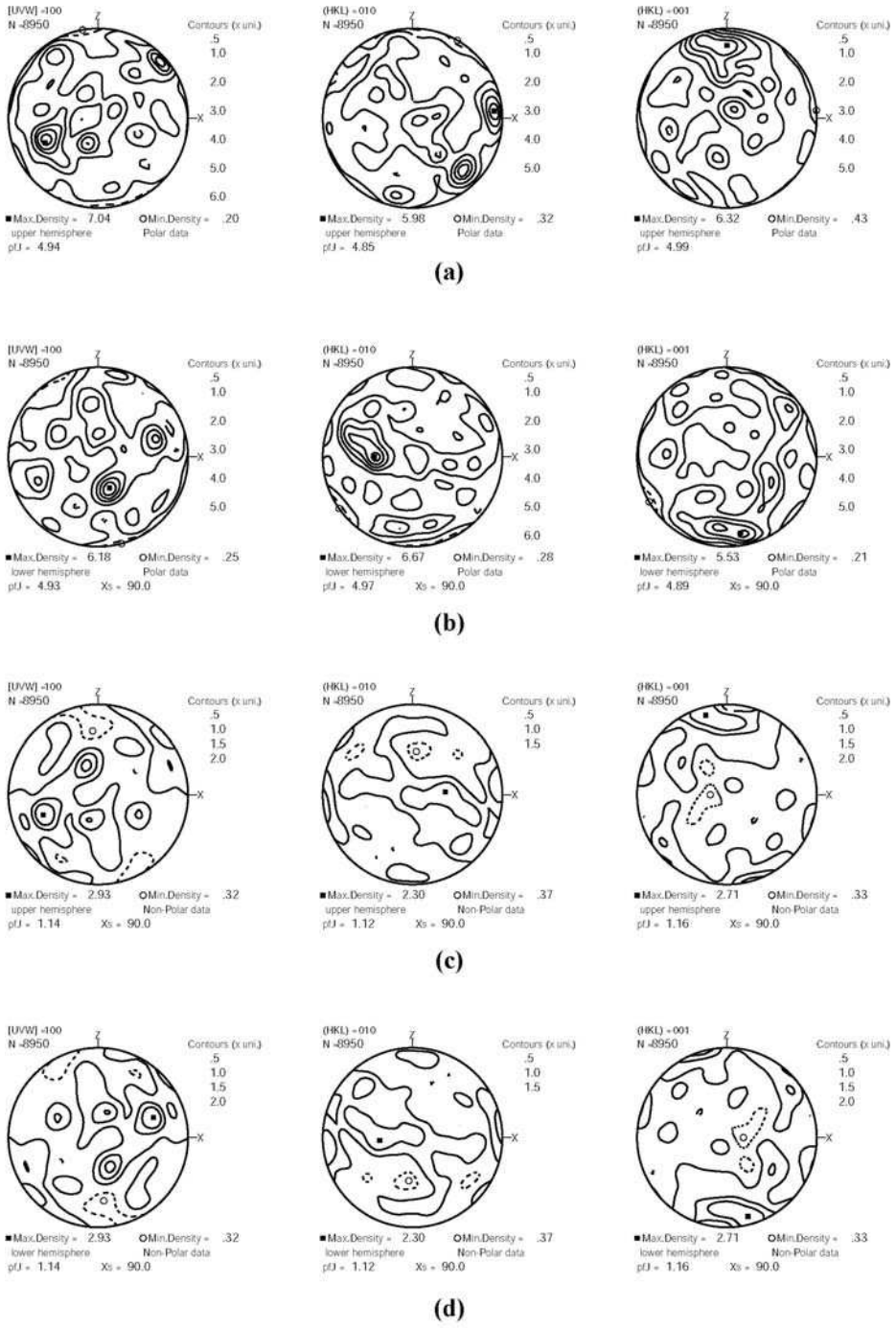

Fig. 5

Figure 5. Equal area projection LPO for plagioclase [100], (010) and (001) orientations illustrating the effect of centro-symmetry and the difference between polar and non-polar data. All contours are multiples of mean uniform distribution (m.u.d.); 0.5m.u.d. contour represented by broken lines; solid square, maximum value; open circle, minimum value. Also shown are values of pfJ for each pole figure. (a) Polar data, upper hemisphere. (b) Polar data, lower hemisphere; note, it is not symmetrically identical to the upper hemisphere plot. (c) Non-polar data, upper hemisphere. (d) Non-polar data, lower hemisphere; note, it is symmetrically identical to the upper hemisphere plot.

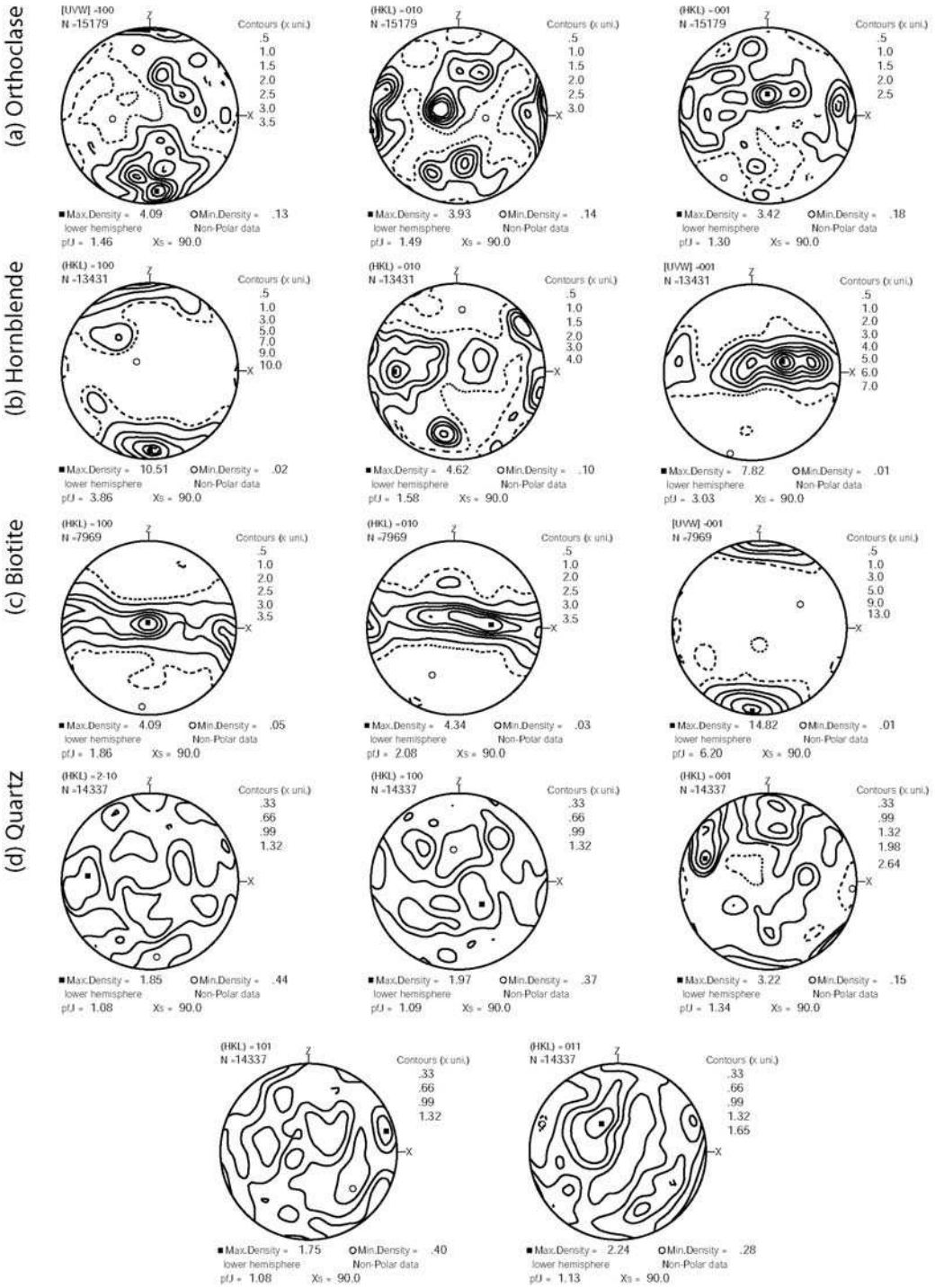

Fig. 6

Figure 6. Individual mineral equal area projection LPO pole figures for sample VPK4. All contours are multiples of mean uniform distribution (m.u.d.); 0.5m.u.d. contour represented by broken lines; solid square, maximum value; open circle, minimum value. Also shown are values of pfJ for each pole figure. (a) Orthoclase [100], (010) and (001). (b) Hornblende (100), (010) and [001]. (c) Biotite (100), (010) and [001]. (d) Quartz $(2\bar{1}\bar{1}0)$, $(10\bar{1}0)$, (0001), $(10\bar{1}1)$ and $(01\bar{1}1)$.

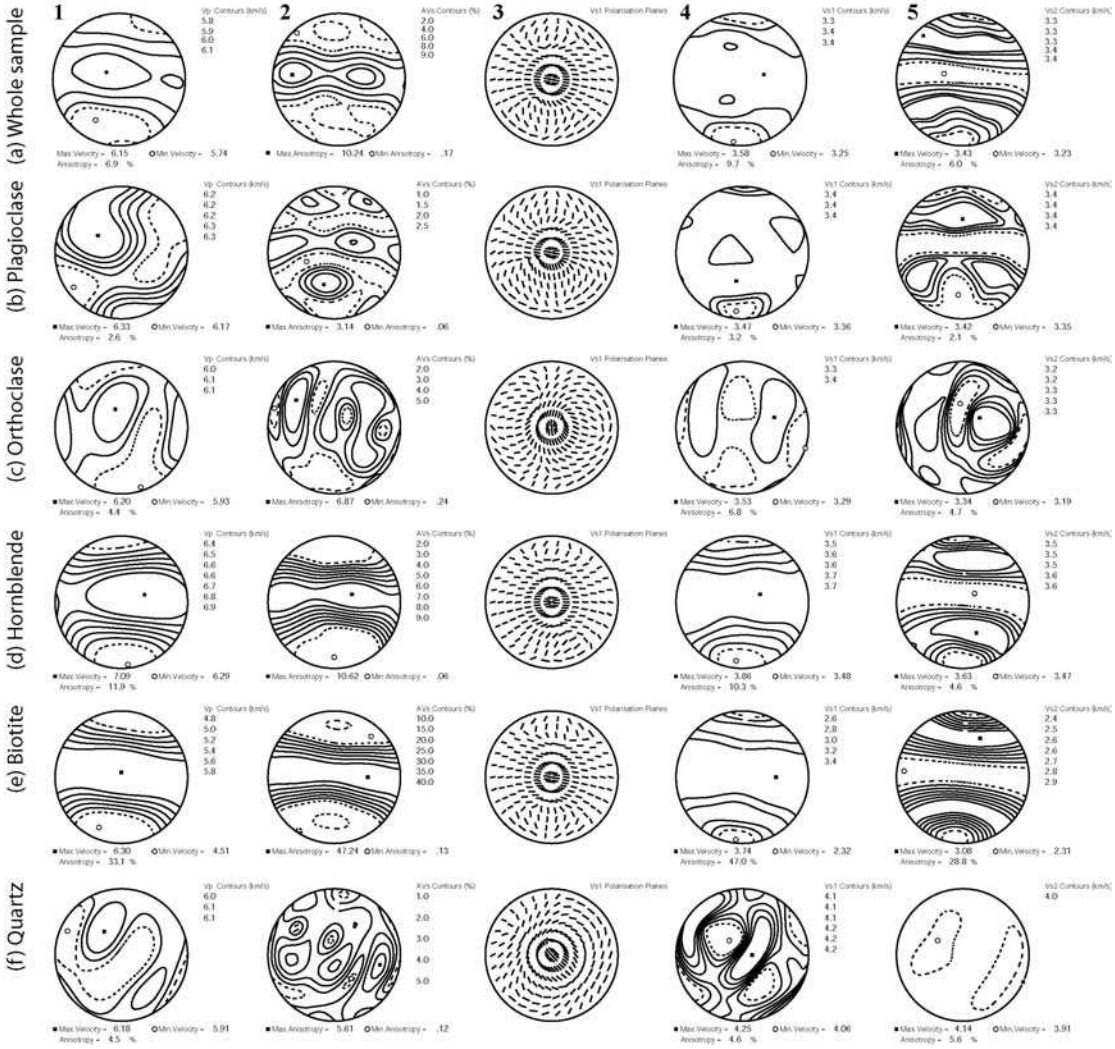

Figure 7. Seismic properties of sample VPK4: 1. compressional wave velocity (Vp km/s) and anisotropy (AVp%); 2. shear wave anisotropy or splitting (AVs %); 3. polarisation of fast shear wave (Vs_1); 4. fast shear wave velocity (Vs_1 km/s) and anisotropy (AVs_1 %); and 5. slow shear wave velocity (Vs_2 km/s) and anisotropy (AVs_2 %). All contours as indicated; solid square, maximum value; open circle, minimum value. (a) Whole sample. (b) Assuming 100% plagioclase. (c) Assuming 100% orthoclase. (d) Assuming 100% hornblende. (e) Assuming 100% biotite. (f) Assuming 100% quartz.

Table 1. Elastic constants for (a) individual single crystals, (b) individual mineral LPO and (c) bulk aggregate.

Phase	(a) Single crystal elastic stiffness	(b) Mineral LPO elastic stiffness (VRH)
plagioclase	**Aleksandrov et al. 1974 VRH - volume average** 0.8200 0.3980 0.4100 0.0001 -0.0840 0.0001 0.3980 1.4500 0.3370 0.0001 -0.0630 0.0001 0.4100 0.3370 1.3280 0.0001 -0.1870 0.0001 0.0001 0.0001 0.0001 0.1810 0.0001 -0.0100 -0.0840 -0.0630 -0.1870 0.0001 0.3100 0.0001 0.0001 0.0001 0.0001 -0.0100 0.0001 0.3350	1.0469 0.4124 0.4141 -0.0042 0.0039 0.0072 0.4124 1.0222 0.4099 -0.0043 -0.0053 0.0091 0.4141 0.4099 1.0382 -0.0096 -0.0094 0.0062 -0.0042 -0.0043 -0.0096 0.3075 0.0009 -0.0058 0.0039 -0.0053 -0.0094 0.0009 0.3000 -0.0003 0.0072 0.0091 0.0062 -0.0058 -0.0003 0.2999
orthoclase	**Alexandrov et al (1974) Microcline Mbars** 0.6700 0.4530 0.2650 0.0005 -0.0024 -0.0018 0.4530 1.6930 0.2040 0.0015 -0.1230 0 -0.0015 0.2650 0.2040 1.1820 -0.0017 -0.1500 0.0004 0.0005 0.0015 -0.0017 0.1430 0.0003 -0.0190 -0.0024 -0.1230 -0.1500 0.0003 0.2380 0.0007 -0.0018 -0.0015 0.0004 -0.0190 0.0007 0.3640	0.9003 0.3582 0.3743 -0.0002 -0.0088 -0.0088 0.3582 0.9726 0.3490 0.0046 0.0061 0.0028 0.3743 0.3490 0.9528 -0.0194 -0.0149 -0.0026 -0.0002 0.0046 -0.0194 0.2644 0.0010 0.0057 -0.0088 0.0061 -0.0149 0.0010 0.2882 0.0025 -0.0088 0.0028 -0.0026 0.0057 0.0025 0.2762
hornblende	**Aleksandrov and Ryzhova 1961 Mbars** 1.1600 0.4990 0.6140 0.0000 0.0430 0.0000 0.4990 1.5970 0.6550 0.0000 -0.0250 0.0000 0.6140 0.6550 1.9160 0.0000 0.1000 0.0000 0.0000 0.0000 0.0000 0.5740 0.0000 -0.0620 0.0430 -0.0250 0.1000 0.0000 0.3180 0.0000 0.0000 0.0000 0.0000 -0.0620 0.0000 0.3680	1.2914 0.5757 0.5854 0.0085 -0.0118 -0.0083 0.5757 1.5489 0.6228 0.0265 -0.0141 -0.0051 0.5854 0.6228 1.6034 0.0158 -0.0400 -0.0018 0.0085 0.0265 0.0158 0.4749 -0.0029 -0.0141 -0.0118 -0.0141 -0.0400 -0.0029 0.3961 -0.0021 -0.0083 -0.0051 -0.0018 -0.0141 -0.0021 0.3956
biotite	**Alexsandrov & Ryzhova 1961** 1.8600 0.3240 0.1160 0.0000 0.0000 0.0000 0.3240 1.8600 0.1160 0.0000 0.0000 0.0000 0.1160 0.1160 0.5400 0.0000 0.0000 0.0000 0.0000 0.0000 0.0000 0.0580 0.0000 0.0000 0.0000 0.0000 0.0000 0.0000 0.0580 0.0000 0.0000 0.0000 0.0000 0.0000 0.0000 0.7680	0.6454 0.2738 0.2591 -0.0072 -0.0019 0.0056 0.2738 1.1075 0.3087 0.0110 -0.0027 0.0569 0.2591 0.3087 1.1949 0.0078 -0.0717 0.0056 -0.0072 0.0110 0.0078 0.3981 0.0300 -0.0289 -0.0019 -0.0027 -0.0717 0.0300 0.1756 -0.0031 0.0056 0.0569 0.0056 -0.0289 -0.0031 0.1711
quartz	**McSkimin et al 1965 alpha quartz d=2.648 g/cm3** 0.8680 0.0704 0.1191 -0.1804 0.0000 0.0000 0.0704 0.8680 0.1191 0.1804 0.0000 0.0000 0.1191 0.1191 1.0575 0.0000 0.0000 0.0000 -0.1804 0.1804 0.0000 0.5820 0.0000 0.0000 0.0000 0.0000 0.0000 0.0000 0.5820 -0.1804 0.0000 0.0000 0.0000 0.0000 -0.1804 0.3988	0.9830 0.0739 0.0857 0.0049 -0.0014 0.0042 0.0739 0.9561 0.0940 0.0198 0.0086 -0.0178 0.0857 0.0940 0.9425 -0.0227 -0.0158 0.0165 0.0049 0.0198 -0.0227 0.4513 0.0196 0.0025 -0.0014 0.0086 -0.0158 0.0196 0.4539 0.0063 0.0042 -0.0178 0.0165 0.0025 0.0063 0.4431
(c) Bulk aggregate		0.9784 0.3575 0.3599 -0.0018 0.0007 -0.0001 0.3575 1.0673 0.3643 0.0062 -0.0018 0.0110 0.3599 0.3643 1.0864 -0.0075 -0.0246 0.0045 -0.0018 0.0062 -0.0075 0.3464 0.0077 -0.0076 0.0007 -0.0018 -0.0246 0.0077 0.2993 -0.0001 -0.0001 0.0110 0.0045 -0.0076 -0.0001 0.2958